Analysis of the impact of parallel magnetic fluctuations on linear gyrokinetic stability in NSTX-U and verification of gyro-fluid models

J. E. Kinsey,[1] G. M. Staebler,[2] E. Belli,[3] and J. Candy[3]

[1)]*CompX, P.O. Box 2672, Del Mar, California 92014, USA*

[2)]*Oak Ridge National Laboratory, Oak Ridge, TN, 37831, USA*

[3)]*General Atomics, P.O. Box 85608, San Diego, California 92186-5608, USA*

(*Electronic mail: staeblergm@ornl.gov)

(Dated: 27 May 2025)

In this work, we use the CGYRO gyrokinetic code to analyze two L- and one H-mode discharges from the National Spherical Torus Experiment (NSTX) and NSTX-Upgrade (NSTX-U) selected due to their different mix of ion-scale driftwaves, ion temperature gradient (ITG) and trapped electron modes (TEM), and electromagnetic instabilities, kinetic ballooning (KBM), and micro-tearing modes (MTM) in the plasma core. It is found that the effect of parallel magnetic fluctuations is strongly destabilizing to the unstable KBMs compared to calculations with only perpendicular magnetic fluctuations. Two discharges have a mix of ITG/TEM and MTMs that are predicted to be dominant instability across the plasma radius. The parallel magnetic fluctuations are found to have little effect on the MTM stability but are destabilizing to ITG/TEM modes. To test the validity of the gyro-fluid linear stability codes TGLF and GFS at low aspect ratio, a database of linear growth rates has been created using the CGYRO gyrokinetic code. The database is comprised of various parameter scans around a standardized set of NSTX-U core parameters. It contains a group of electrostatic cases and an electromagnetic group that includes the effects of perpendicular and parallel magnetic fluctuations. Comparing the results from the GFS and TGLF models, we find that GFS exhibits the best agreement with the database of CGYRO linear growth rates. Comparing the model results for the electromagnetic scans shows that GFS captures the effects of parallel magnetic fluctuations accurately, while the TGLF model does not, as it lacks sufficient perpendicular energy resolution.

PACS numbers: 52.65.-y,52.25.Fi,52.55.Fa

I. INTRODUCTION

Tokamak transport has long been observed to be anomalous in nature and, in plasmas lacking large scale MHD instabilities, believed to be largely governed by driftwave instabilities with ion temperature gradient (ITG) and trapped electron modes (TEM) as the leading cause of the radial density and energy transport in the plasma core region. At electron scales the electron temprature gradient is also a contributor to mostly electron energy transport. Historically, the emphasis on reduced transport model development has been on creating quasi-linear models that capture the physics of ITG and TEM modes and calibrating the results against gyrokinetic simulations. Both the development and validation of driftwave transport models have focused on conventional tokamak scenarios with aspect ratios in the vicinity of $R/a = 3$. The fusion community has witnessed significant progress over the last two decades with transport models evolving from formula based models to gyro-Landau fluid eigenmode based models. Quasi-linear transport models can use linear eigenmodes from gyrokinetic turbulence simulation codes[1,2] but the reduced fluid models compute approximate eigenmodes much faster. The Trapped Gyro-Landau-Fluid (TGLF) model[3–5] was developed and verified against a database of electrostatic gyrokinetic simulations. The quasi-linear transport model using TGLF eigenmodes has also been successfully validated against a variety of experimental data from DIII-D, JET, TFTR, and ASDEX-Upgrade tokamaks[6–9]. However, very little attention has been given to testing the accuracy of TGLF linear eigenmodes against gyrokinetic linear stability from low aspect ratio (R/a¡2) devices such as NSTX[10], NSTX-U[11], MAST[12] and MAST-U[13].

Gyrokinetic studies of low aspect ratio tokamak plasmas have found that the instability spectrum is more complicated than what is typically found in conventional tokamaks. In addition to ITG/TEM and electron scale electron temperature gradient (ETG) modes, theoretical studies have suggested that kinetic ballooning (KBM)[14–16] and micro-tearing (MTM) modes[17–21] could be playing a role in low aspect ratio tokamaks. Recent analyses of NSTX-U discharges have shown that indeed the electromagnetic branches, KBMs and MTMs, are found to be unstable[22–25]. Furthermore, studies have shown that the electromagnetic effects of magnetic perturbations both perpendicular and parallel to the equilibrium magnetic field can be important[26]. Non-linear turbulence simulations have found that transport due to MTMs is greatly suppressed when equilibrium $E \times B$ velocity shear is taken into account[27].

In this paper, we use the CGYRO code[28–30] for linear gyrokinetic analysis of three L- and H-

mode discharges selected to illustrate the range of instabilities found in previous linear gyrokinetic analysis. One goal is to examine the relative stability of ITG/TEM, KBM, and MTM in the plasma core. We focus on the role of parallel magnetic field fluctuations for these instabilities. The parallel magnetic field fluctuations ($\tilde{B}_{||}$) are driven by the perpendicular pressure gradient current and hence have the same parity and a stronger coupling to the electric potential fluctuations ($\tilde{\phi}$) than the perpendicular magnetic fluctuations ($\tilde{B}_{\perp}$) driven by parallel currents. In analyzing each case with CGYRO we aim to gain new insights and assess the relative roles of $\tilde{B}_{||}$ effects on the unstable modes. It is found that the KBM branch is destabilized by parallel magnetic fluctuations but the MTM branch is insensitive to $\tilde{B}_{||}$. Perhaps this difference could be due to the change in electric potential $\tilde{\phi}$ wavefunction parity, with KBM having even parity and MTM having odd parity along the magnetic field line.

We also compare the CGYRO results to the gyro-fluid models, TGLF[4] and GFS[31] for the same three discharges. A primary goal of this work is to verify the accuracy and parametric dependence of the gyro-fluid models, for low aspect ratio. A systematic test of the models is made using a database of linear growth rates and mode frequencies assembled from CGYRO runs. The database is comprised of parameter scans around a standard case based on NSTX-U core parameters. We test the models against the database which is split into a set of electrostatic (ES) scans ($\tilde{\phi}$), partial electromagnetic scans (EM1) with just ($\tilde{\phi}, \tilde{B}_{\perp}$), and fully electromagnetic scans (EM2) with both magnetic fluctuation components ($\tilde{\phi}, \tilde{B}_{\perp}, \tilde{B}_{||}$).

II. GYROKINETIC ANALYSIS OF NSTX AND NSTX-U DISCHARGES

In this section, we summarize the results of performing various linear gyrokinetic simulations using the CGYRO code for three discharges. Here we examine the relative roles of ion-scale ITG/TEM modes, kinetic ballooning modes (KBMs), and micro-tearing modes (MTMs). Included in the results is an analysis of the impact of perpendicular magnetic perturbations ($\tilde{B}_{\perp}$) and parallel magnetic perturbations ($\tilde{B}_{||}$) in the CGYRO calculations.

A. Gyrokinetic Analysis of NSTX L-mode #141716

We first focus on NSTX low confinement (L-mode) discharge #141716 which was recently studied using the TGLF model[32]. This discharge has the following parameters: magnetic field

B_T=0.54 T, plasma current I_p=0.90 MA, aspect ratio R/a=0.85/0.65 m, and neutral beam injected heating power P_{NBI}= 2 MW, and a line-averaged electron density of $\bar{n}_e = 3\times10^{19}/m^3$. This discharge was originally reported on in Ref.[33] and was also analyzed using the GS2[34] gyrokinetic code.

Using the CGYRO code, with Miller equilibrium[35], we first performed linear runs across the radius with a focus on ion-scale modes. The resolution settings used for CGYRO are 8 energy quadrature points with a maximum energy of 8, 18 pitch angle points, 24 poloidal angle grid points per period and 12 periods. This was determined to be sufficient accuracy to find even MTM modes. A pure plasma with deuterium ions is used. Impurity and fast ions were not included. The CGYRO runs were carried out both with electrostatic (ES) and electromagnetic (EM) effects. For ideal MHD theory, there is a well-known cancellation of the pressure contribution to the magnetic grad-B drift due to parallel magnetic flutter generated by the perpendicular pressure gradient fluctuation[36]. Hence setting the grad-B drift = curvature drift (MHD rule), neglecting the pressure gradient contribution to the grad-B drift, is a good approximation for linear ideal MHD without including the parallel magnetic field fluctuations. For gyrokinetic theory, a partial cancellation still exists but it is not as good an approximation to simply set the pressure gradient term in the grad-B drift to zero and neglect the parallel magnetic flutter[16] especially for low aspect ratio. Our purpose is to test the impact of parallel magnetic flutter not to repeat test of this MHD rule approximation[26]. Parallel magnetic field fluctuations drive quasi-linear (and non-linear) fluxes so a fully electromagnetic gyrokinetic calculation is required to compute the total fluxes. The pressure gradient contribution to the MHD equilibrium and the magnetic drifts is retained for all figures.

Figure 1 shows the linear growth rates versus radius for #141716 at a normalized poloidal wavenumber of $k_y = 0.3$ where $k_y = k_\theta \rho_s$, $k_\theta = nq/r$, $\rho_s = c_s m_i c/eB_{unit}$, $c_s = \sqrt{T_e/m_i}$, $B_{unit} = (q/r)d\psi/dr$, $n =$ toroidal mode number, and $2\pi\psi =$ poloidal magnetic flux. This is often near the ion-scale maximum of the linear growth rate. Shown are the ES results ($\tilde{\phi}$) only (gray dashed) and the EM1 results with ($\tilde{\phi}, \tilde{B}_\perp$) only (gray) and EM2 ($\tilde{\phi}, \tilde{B}_\perp, \tilde{B}_{||}$) (black) fluctuations. Beyond $r/a = 0.50$, comparing the gray (EM1) and black (EM2) curves shows that finite β effects of $\tilde{B}_{||}$ are destabilizing, cancelling out the stabilizing effect of $\tilde{B}_\perp$ on the ITG/TEM modes relative to the ES (gray dashed) case. A new branch appears near $r/a = 0.3$ that is strongly destabilized by $\tilde{B}_{||}$. The large negative mode frequency in Fig. 1b is consistent with these modes being KBMs propagating in the ion diamagnetic direction.

Figure 2 compares the EM2 growth rates versus the Waltz[37] $E\times B$ shear rate $\gamma_{E\times B} = (r/q)d(cE_r/(RB_p))/dr$

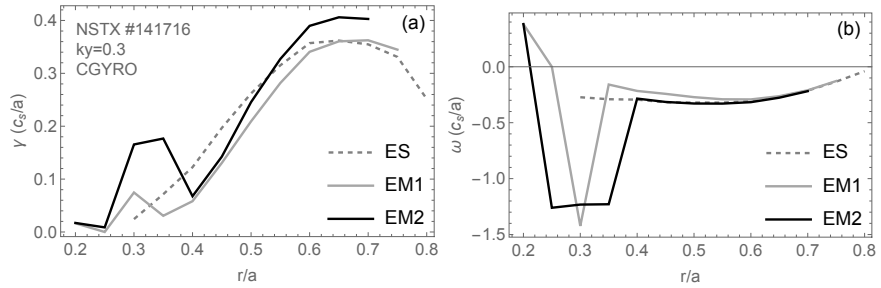

FIG. 1. Growth rate (a) and frequency (b) vs radius for NSTX #141716 using CGYRO. Shown are three cases: ES $\tilde{\phi}$ (gray dashed), EM1 ($\tilde{\phi}, \tilde{B}_\perp$) (gray), and EM2 ($\tilde{\phi}, \tilde{B}_\perp, \tilde{B}_{||}$) (black).

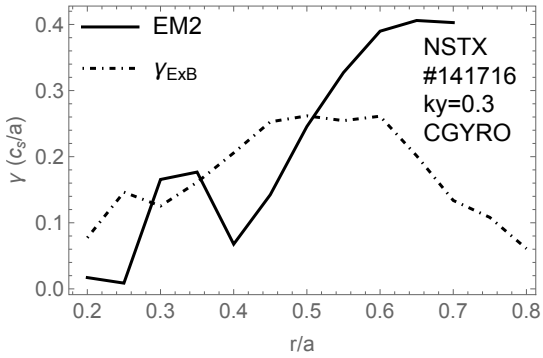

FIG. 2. The CGYRO EM2 growth rate (black) compared to the $E \times B$ shear rate (dot-dashed) for L-mode #141716.

across the radius. The $E \times B$ shear is significant, and mostly exceeds the growth rate out to a minor radius of $r/a = 0.50$ (r/a = RMIN in CGYRO). However, the KBM around $r/a = 0.30$ has a growth rate that exceeds the $E \times B$ shear due to enhancement by the $\tilde{B}_{||}$ fluctuations. The enhanced KBM growth rate by $\tilde{B}_{||}$ fluctuations is consistent with previous studies[15,16]. Here, the growth rates at $k_y = 0.30$ more than double when $\tilde{B}_{||}$ is included in the CGYRO calculations.

Figure 3 shows the growth rates versus electron beta β_e for #141716 at $r/a = 0.30$ predicted by CGYRO with only $\tilde{B}_\perp$ included (EM1) (gray) and both $\tilde{B}_\perp$ and $\tilde{B}_{||}$ (EM2) (black). Here, $\tilde{\phi}$ remains even parity while $\tilde{B}_\perp$ remains odd parity across the ballooning limit. Below the ballooning threshold ITG modes dominate and both the real and imaginary parts of $\tilde{B}_\perp$ are in phase with each other. Above the threshold, KBM modes dominate and, like ITG modes, propagate in the ion diamagnetic drift direction. Just above the threshold, the growth rates increase rapidly with β_e

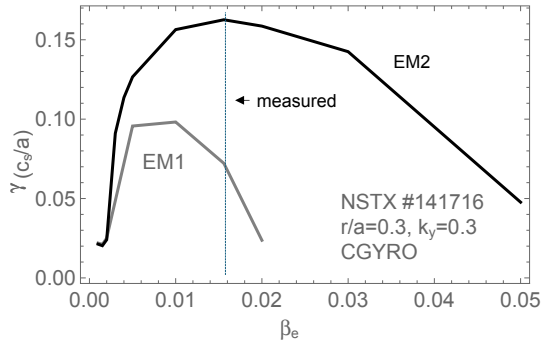

FIG. 3. Growth rate vs β_e for NSTX #141716 at ρ=0.30. EM1 ($\tilde{\phi}, \tilde{B}_\perp$) (gray) and EM2 ($\tilde{\phi}, \tilde{B}_\perp, \tilde{B}_{||}$) (black) using CGYRO.

and the real and imaginary parts of $\tilde{B}_\perp$ become increasingly out of phase with each other. The measured experimental β_e value is indicated by the vertical dashed line in Fig. 3. Examining the $\tilde{B}_{||}$ enhanced KBM in #141716 at $r/a = 0.3$ shows that while $\tilde{\phi}$ is even parity as expected, it has a oscillatory structure, and is extended in ballooning angle ($\theta_{\max} = 10\pi$). This is typical of weak magnetic shear regions.

B. Gyrokinetic Analysis of NSTX-U L-mode #204551

In this subsection, we summarize the results of analyzing an NSTX-U L-mode discharge #204551. The parameters for this discharge are: B_T=0.66 T, I_p=0.79 MA, R/a=1.04/0.57 m, $P_{\mathrm{NBI}} \approx 2.5$ MW, and a line-averaged electron density of $\bar{n}_e \approx 5 \times 10^{19}/m^3$. This discharge was originally reported on, and analyzed using the GYRO code, in Ref.[23].

Figure 4 shows the linear growth rates versus radius for NSTX-U discharge #204551 at a wavenumber of $k_y = 0.3$. Similar to L-mode #141716, the effects of $\tilde{B}_\perp$ alone (gray) are stabilizing compared to ES (gray dashed) while adding $\tilde{B}_{||}$ (black) is closer to the ES curve for ITG/TEM modes at large radii ($\rho > 0.6$). Unlike #141716, MTMs are dominant at inner radii instead of KBMs. The MTMs are EM modes so are not predicted for the ES curve (gray dashed). With $\tilde{B}_\perp$ included, MTMs dominate inside $r/a = 0.55$ which is in agreement with previous GYRO results[23]. Adding in the effects of $\tilde{B}_{||}$, we observed very little change in the MTM growth rates with the black and gray curves overlapping.

Unlike KBM modes, the MTM electrostatic potential is odd parity (anti-symmetric about

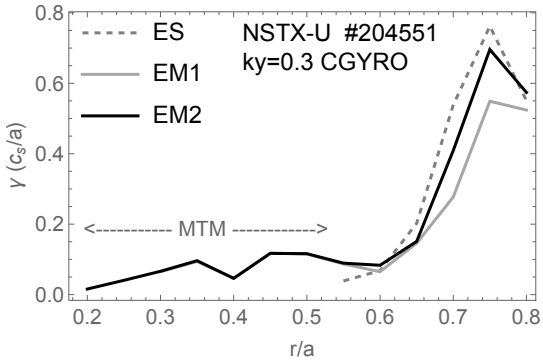

FIG. 4. Growth rate vs radius for NSTX-U #204551 using CGYRO ES (gray dashed), EM1 (gray) and EM2 (black).

$\theta = 0$) and $\tilde{B}_\perp$ is even parity (tearing parity). Figure 5 shows the CGYRO wavefuntion of the MTM at $r/a = 0.55$ and $k_y = 0.30$ with the electric potential $\tilde{\phi}$ (top) and the transverse magnetic fluctuations ($\tilde{A}_{||} = \tilde{B}_\perp / k_\perp$) (bottom) plotted versus extended ballooning angle. Both the real (black) and imaginary (gray) parts are shown. Examining the spectra at this radius, we find that MTMs are dominant over a large range spanning $0.1 \leq k_y \leq 0.5$. At larger k_y, TEM and eventually electron temperature gradient (ETG) modes become dominant.

After analyzing discharge #204551, a sensitivity study was performed comparing the local parameters for the 2 L-modes. Here, the motivation was to investigate why one discharge was KBM dominant and the other was MTM dominant. We focused on a radius of $r/a = 0.30$. At that radius, with EM2 effects included, in CGYRO, #141716 is KBM dominant while #204551 is MTM dominant. The sensitivity to four key parameters was tested for #141716 and #204551 including ion temperature gradient length a/L_{T_i}, electron-ion collision frequency $\nu_{e,i}$, magnetic shear $\hat{s}$, and electron density gradient length a/L_{n_e}. Starting from the parameters in #204551, each quantity was varied and the impact on the MTM was observed. The key parameters that had the largest impact were a/L_{T_i} and a/L_{n_e}. Once a/L_{T_i} was increased from 1.2 to 2.5, only a very small increase in a/L_{n_e} was required for the dominant mode to switch from MTM to KBM. This suggests that, at low power (and low a/L_{T_i}), MTMs may dominate in the core region, but as the ion heating power is increased (and a/L_{T_i} increases) KBMs or ITG/TEM modes will become dominant. This, of course, assumes the local conditions are sufficient in order to drive an MTM, in particular, the electron beta and collision frequency as pointed out in Ref.[23].

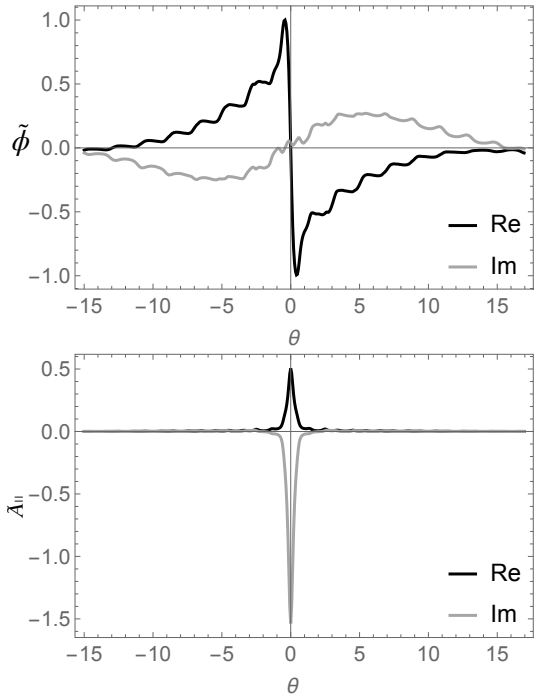

FIG. 5. Real (black) and imaginary (gray) parts of the electric potential ($\tilde{\phi}$) (top) and perpendicular magnetic $\tilde{A}_{||} = \tilde{B}_{\perp}/k_{\perp}$ (bottom) fluctuations vs ballooning angle for the MTM at $r/a = 0.55$ with $k_y = 0.3$ in #204551.

C. Gyrokinetic Analysis of NSTX H-mode #121009

The last discharge we analyze is the NSTX high confinement (H-mode) discharge #121009 which has the following parameters: B_T=0.55 T, I_p=1.07 MA, R/a=0.83/0.59 m, and P_{NBI}= 1.7 MW, and a line-averaged electron density of $\bar{n}_e = 4.4 \times 10^{19}/m^3$. The profiles are analyzed using CGYRO at a time slice of 300 ms. In analyzing the low-k modes we find that MTMs are the dominant mode across nearly the entire radius out to $r/a = 0.70$. Unlike the L-mode discharges, ITG/TEM modes are either stable or subdominant when electromagnetic effects are included. Figure 6 shows the linear growth rates versus radius for $k_y = 0.30$. The ES results (gray dashed) have only a small region of ITG/TEM instability $0.65 \leq \rho \leq 0.75$. In this region, the EM1 curve (gray) shows a reduced ITG/TEM growth rate at $r/a = 0.75$ and a weak KBM at $r/a = 0.80$. The KBM growth rate is greatly enhanced for $\rho \geq 0.75$ by the EM2 (black) inclusion of $\tilde{B}_{||}$.

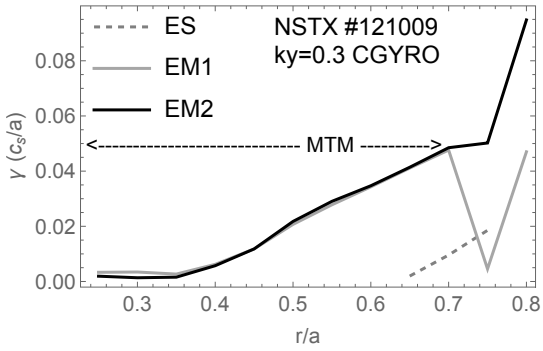

FIG. 6. Growth rate vs radius for NSTX-U H-mode #121009 using CGYRO ES (gray dashed), EM1 (gray) and EM2 (black).

The MTM branch is dominant over the region $0.25 \leq \rho \leq 0.70$ for both of the EM cases with little impact of $\tilde{B}_{||}$ on the growth rates. We note that the ion temperature gradient scale length, a/L_{T_i}, is relatively low across the plasma in #121009 and is indicative of low ion heating. One can speculate, based on the analysis of discharge #204551, that as more NBI heating is added then a/L_{T_i} would increase and ITG/TEM and/or KBMs would become the dominate unstable modes. This hypothesis has not been tested.

III. VERIFICATION OF THE TGLF AND GFS MODELS FOR TWO EXPERIMENTAL DISCHARGES

In this section we compare the linear growth rates from the TGLF model versions (SAT1 and SAT2) against the linear CGYRO results for the previously examined discharges. These model versions refer to different models for the saturated electric potential fluctuations used to compute fluxes. However, the electron collision model and loss of bounce averaging models also differ and this impacts the linear eigenmodes. The Trapped Gyro Landau Fluid (TGLF) equations[3] have bounce averaged trapped particles (3 moments) and circulating particles (12 moments) with a generalization of the 6 moment Beer-Hammett closure scheme[38] with closure coefficients that depend on the fraction of trapped particles. The TGLF equations do not have enough perpendicular energy moments to compute the energy flux and Reynolds stress due to parallel magnetic fluctuations. The linear growth rates of TGLF were shown to agree with the gyrokinetic growth rates of Kotschenreuther's GKS code[34] to within 11.4% for a large database of collisionless cases. The

pitch angle scattering collisions in TGLF require modeling the gradient of the distribution function at the trapped-passing boundary. The SAT1 model for collisions was tuned[5] to the GYRO code[39] The SAT2 model for collisions re-tuned this trapped passing boundary model[1] to the CGYRO code[28] and added a model for the gradual loss of bounce averaging as the diamagnetic drift frequency exceeds the transit frequency. Only the TGLF-SAT2 grwothrates will be compared with CGYRO in the analysis of the two selected discharges.

We compliment the TGLF results with results from the newly developed GFS model which is an improvement in velocity space resolution over TGLF. The Gyro Fluid System (GFS) model[31] uses a real two parameter closure and does not impose bounce averaging of trapped particles. Pitch angle scattering collisions are included in GFS without the need to model the trapped-passing boundary layer that was required for TGLF. The GFS equations are moments of the symmetric Sugama-Horton form[40] of the gyrokinetic equations. The GFS equations preserve the Onsager symmetry of the flux-gradient matrix. The GFS equations have a variable number of velocity moments. For this paper, three perpendicular energy and seven parallel velocity moments were used. This resolution was found to be optimal for the SAT2 database of CGYRO runs that centers on $R/a = 3.0$ aspect ratio[31]. This paper is the first broad test of GFS for low aspect ratio and experimental conditions. Both TGLF and GFS use a Hermite polynomial moment representation for the along-the-field wavefunction. TGLF has a two-step solution method with a variable width for the Gaussian envelope chosen to maximize the 2 moment growth rate, that is then refined at fixed width with 4 (for SAT1) or 6 (for SAT2) moments. The GFS eigenmodes use a fixed envelope width (1.74) and 12 Hermite polynomial moments that was found to yield good accuracy compared to CGYRO for this velocity resolution for the database of CGYRO runs used to fit SAT2. Using the Hermite polynomials gives fast, accurate, toroidal drift-ballooning eigenmodes (ITG, TEM, ETG, KBM). At least three perpendicular energy moments in GFS are needed in order to calculate the particle flux, energy fluxes and the toroidal Reynolds stress due to parallel magnetic field fluctuations. The importance of the parallel magnetic fluctuations for the kinetic ballooning mode (KBM) stability in NSTX-U that was found for CGYRO will be shown to be better captured by GFS than either of the TGLF versions.

In our analysis, we exclude any comparisons where CGYRO predicts microtearing modes (MTMs) as the dominant instability. Both models were found to not be able to capture the MTM two-scale wavefunctions displayed in Fig. 5. This is attributed to the use of Hermite basis functions for the parallel wavefunction, that are adapted to ballooning type modes, in both fluid codes.

It is planned to add a parallel grid, like in CGYRO, to GFS to enable MTM resolution. Previously, it was shown that CGYRO predicted that MTMs dominate over most of the radius in discharge #121009. Therefore, we will exclude that case and focus on the other two discharges in the regions where CGYRO predicts ITG and KBM modes.

Comparison of the CGYRO linear growth rate (black) for the L-mode discharge #141716 with TGLF-SAT2 (gray dashed) and GFS (gray) in Fig. 7, we find that TGLF and GFS predict similar growth rates for the region between $r/a = 0.45$ and $r/a = 0.60$. In that region, both models show good agreement with CGYRO. Inside $r/a = 0.45$, KBMs dominate. The large effect of $\tilde{B}_{||}$ on the KBM at $r/a = 0.30$ was demonstrated in Fig. 1. Comparing the model predictions, we find that GFS demonstrates better agreement with CGYRO for EM2 because it captures the $\tilde{B}_{||}$ destabilization of the KBM shown in Fig.1 and TGLF EM2 does not. Here, the EM2 effects on the TGLF growth rates is relatively small which is consistent with the analysis performed in Ref.[32]. Outside of $r/a = 0.60$, where ITG modes are dominant, we also observe different results from the two models. This is notable around $r/a = 0.70$ where GFS slightly underpredicts the CGYRO growth rate while TGLF matches the CGYRO result.

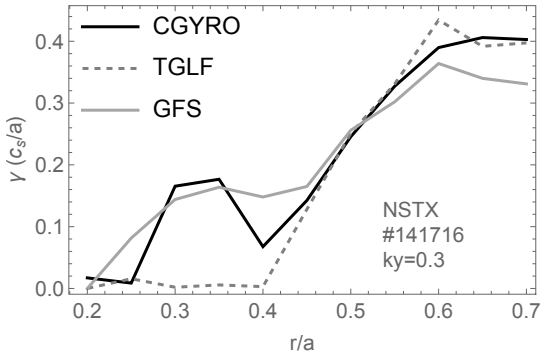

FIG. 7. Growth rate vs radius for NSTX-U L-mode #141716 EM2: CGYRO (black), TGLF-SAT2 (gray dashed) and GFS (gray).

In analyzing the TGLF and GFS results for the NSTX-U discharge #204551, it is found in Fig. 8 that the EM2 growth rates at $k_y = 0.30$ for GFS (gray) are in good agreement with CGYRO (black), whereas TGLF-SAT2 (gray dashed) noticeably under predicts the growth rates inside of $r/a = 0.65$. Thre is a small under prediction by GFS for $r/a \approx 0.75$. Here, analysis was restricted outside of $r/a = 0.50$ where ITG modes are dominant and MTMs are either subdominant or not

unstable.

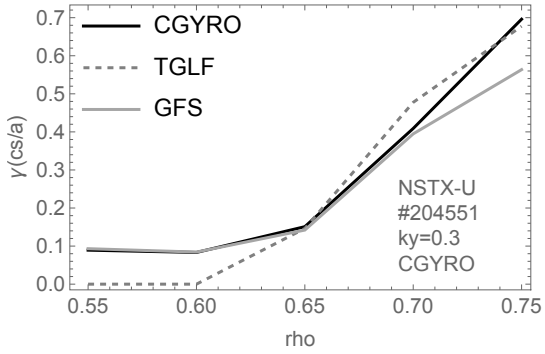

FIG. 8. Growth rate vs radius for NSTX-U #204551 EM2 : CGYRO (black), TGLF-SAT2 (gray, dashed) and GFS (gray).

The k_y spectrum of EM2 linear growth rates for CGYRO (black), TGLF-SAT2 (gray dashed) and GFS (gray) are compared in Fig. 9 for discharge #204551 at $r/a = 0.60$. As evident in Fig. 9, we see that GFS shows better agreement than TGLF below $k_y = 1.0$. However, we find that the accuracy of GFS is degraded for the intermediate k_y and low-k ETG modes above $k_y = 1.0$ in this case. This could be due to the effect of the FLR corrections to the pitch angle scattering electron collisions that are included in CGYRO (full multi-species collisions) but not in GFS. The FLR correction scales like k_y^2 so it will have a larger impact at higher k_y.

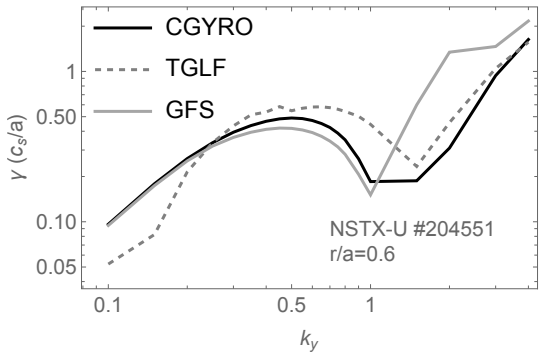

FIG. 9. growth rate vs wavenumber k_y for NSTX-U L-mode #204551 at $r/a = 0.60$ EM2 : CGYRO (black), TGLF-SAT2 (gray, dashed) and GFS (gray).

While a comparison of the gyro-fluid models was useful for the three NSTX-U discharges, we

are motivated to examine the validity of the models over a broader range of parameter space. To carry this out, a database of CGYRO linear gyrokinetic growth rates was assembled using NSTX-U relevant parameters. In the next section, we discuss this database and report on how the TGLF and GFS models compared.

IV. VERIFICATION OF THE TGLF AND GFS MODELS AGAINST A LOW ASPECT RATIO LINEAR GYROKINETIC DATABASE

In this section, we summarize the results of testing the accuracy of the linear growth rates and mode frequencies predicted by TGLF-SAT1, TGLF-SAT2 and GFS against a database of CGYRO gyrokinetic results. The database of CGYRO growth rates is comprised of parameter scans around a standardized case relevant to NSTX-U. The format of the database and testing procedure is similar to what was employed during the development of TGLF whereby scans were performed using the GKS code with parameter scans around the GA STD case[3]. We breakdown the database into 3 parts, an electrostatic part and two electromagnetic parts that include the effects of partial (EM1) and full (EM2) electromagnetic fluctuations.

In this verification study, we construct a new standard (STD) case based on NSTX-U local parameters. For the NSTX-U STD case, the local parameters from #204551 at $r/a = 0.60$ were used and the parameters were rounded off for simplicity. The parameters are as follows (see Ref. 34 for the definitions) : $R/a = 1.75$, $r/a = 0.6$, $q = 1.5$, $\hat{s} = 1.0$, $\kappa = 1.5$, $s_\kappa = -0.1$, $\delta = 0.0$, $s_\delta = 0.0$, $a/L_{T_i} = a/L_{T_e} == a/L_T = 3.0$, $a/L_{n_e} = a/L_{n_i} == a/L_n = 1.0$, $\nu_{e,i} = 1.0$, $\beta_e = 0.005$. For each parameter scan, an ascii file is created whereby the growth rates and mode frequencies from CGYRO are stored. A stand-alone code was created that reads in the CGYRO files and calls the gyrofluid (GF) models, TGLF and GFS, for a particular scan. The growth rates and frequencies are calculated and the RMS errors between the models and CGYRO is then found. An average error is also computed for each scan. The goal is to assess the overall accuracy of both models and reveal where they differ. In testing TGLF, we examine the SAT1 and SAT2 versions of the linear model. Recall that the SAT2 linear collision and loss of bounce averaging models are different than the SAT1 version. The SAT1 model was calibrated with GYRO and the SAT2 version[1] was calibrated with CGYRO using the GA-STD database.

A. Results for the Electrostatic Scans

TABLE I. Linear Electrostatic Gyrokinetic Database for the NSTX-U STD Case

Scan	Parameters	Scan Type	No. Cases
51	NSTX-U STD	k_y @ $q = 1.5, 2.0, 3.0$	22
52	NSTX-U STD	k_y @ $a/L_T = 3.0, 4.0, 5.0$	24
53	NSTX-U STD	$\hat{s}$ @ $q = 1.5, 2.0, 2.5, 3.0$	16
54	NSTX-U STD	q @ $r/a = 0.3, 0.6$	13
55	NSTX-U STD	a/L_T @ $a/L_n = 0.5, 1.0, 1.5, 2.0$	28
56	NSTX-U STD	$\nu_{e,i}$ @ $k_y = 0.15, 0.30$	17
57	NSTX-U STD	r/a @ $R/a = 1.50, 1.75$	14
Total			134

Here, we summarize the results of testing the two versions of TGLF and the new GFS model against the electrostatic (ES) part of the CGYRO database. Only the effects of fluctuations in the electrostatic potential ($\tilde{\phi}$) are included with $\beta_e = 0$. Table 1 lists the various scans in this ES database. There are 7 scan types around the NSTX-U STD case with a total of 134 linear runs. The spectrum is limited to a maximum wavenumber of $k_y = 0.8$ and we do not include the effects of impurities, fast ions or equilibrium velocity gradients. The focus here is on testing the accuracy of TGLF and GFS for the ion scale ES modes ITG/TEM. Overall, the GFS model exhibits the best agreement with the CGYRO results with an average RMS error of 15.7%. TGLF-SAT1 has an average RMS error of 44.4% while TGLF-SAT2 shows better agreement with a RMS error of 32.2%. Figure 10 plots the average RMS error in the growth rates for each ES scan. GFS shows improved agreement over both TGLF models for this database except for scans 53 and 57 where TGLF-SAT2 and GFS are comparable. Comparing the two versions of TGLF, and GFS for a scan in collision frequency $\nu_{e,i}$ (scan 56) in Fig. 11 shows that GFS shows better agreement with CGYRO. We remind the reader that $\nu_{e,i} = 1.0$ is the baseline NSTX-U STD value.

B. Results for the Electromagnetic Scans

In this subsection, we report on results of comparing TGLF and GFS for the CGYRO electromagnetic database. This database, given in Table 2, is split into two sets of scans. The first subset of scans EM1 (58-64) are scans around the NSTX-U STD case including EM1 effects of just potential and perpendicular magnetic fluctuations ($\tilde{\phi}, \tilde{B}_\perp$). The second subset EM2 (65-70) is comprised of EM2 scans that include both the perpendicular and parallel ($\tilde{\phi}, \tilde{B}_\perp, \tilde{B}_\parallel$) magnetic

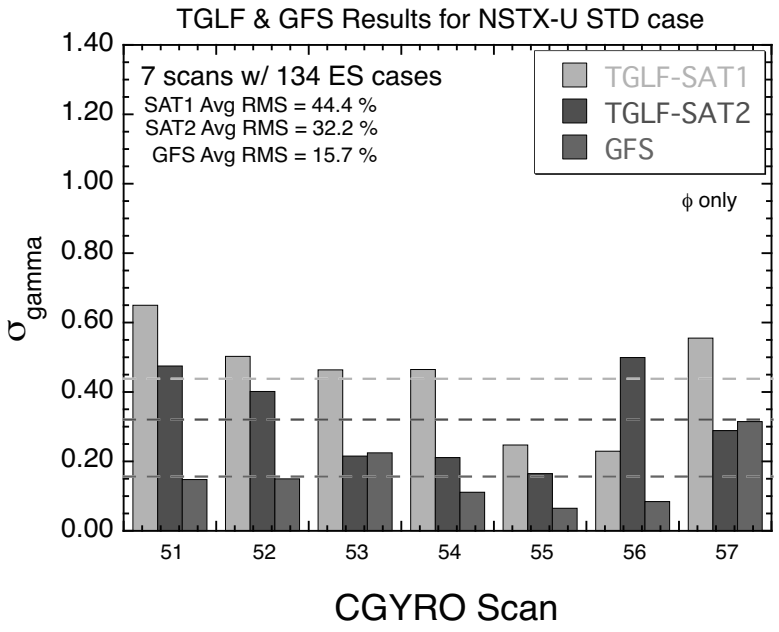

FIG. 10. RMS error in the TGLF growth rates vs scan number for the CGYRO linear database comprised of ES scans around the NSTX-U STD case parameters.

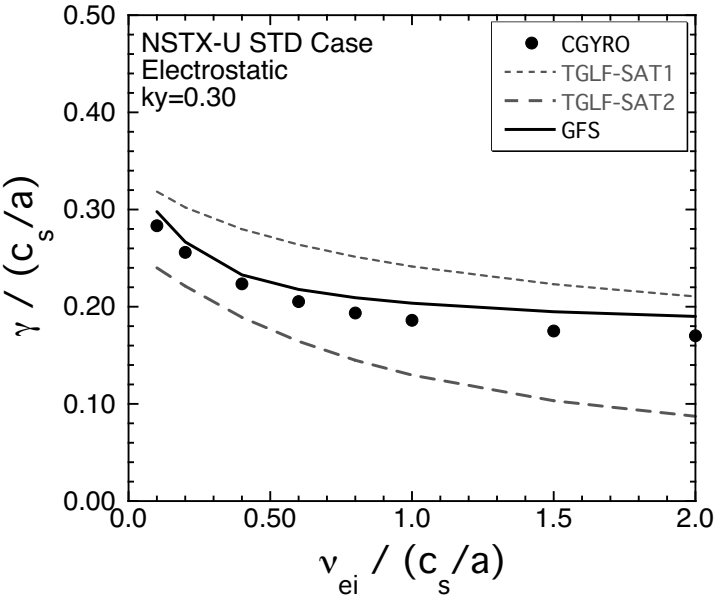

FIG. 11. Growth rate vs collision frequency $(\nu_{ei}/(c_s/a)$ for NSTX-U STD case ES scan #56. The dots denote the CGYRO results and the lines denote the TGLF and GFS results.

TABLE II. Linear Electromagnetic Gyrokinetic Database for the NSTX-U STD Case

Scan	Parameters	Scan Type	No. Cases
58	NSTX-U STD	β_e @ $\hat{s} = 1.0, 1.5$, $\tilde{B}_{\rm per}$ only, w/o p'	19
59	NSTX-U STD	β_e @ $\hat{s} = 0.5, 1.0, 1.5, 2.0$, $\tilde{B}_{\rm per}$ only	20
60	NSTX-U STD	k_y @ $q = 1.5, 3.0$, $\beta_e = 0.005$, $\tilde{B}_{\rm per}$ only	19
61	NSTX-U STD	a/L_T @ $a/L_n = 0.5, 1.0, 2.0$, $\beta_e = 0.005$, $\tilde{B}_{\rm per}$ only	18
62	NSTX-U STD	$\hat{s}$ @ $q = 1.5, 2.0, 2.5$, $\beta_e = 0.005$, $\tilde{B}_{\rm per}$ only	13
63	NSTX-U STD	q @ $\beta_e = 0.001, 0.005$, $\tilde{B}_{\rm per}$ only	14
64	NSTX-U STD	$\nu_{e,i}$ @ $k_y = 0.15, 0.30$, $\beta_e = 0.005$, $\tilde{B}_{\rm per}$ only	17
65	NSTX-U STD	β_e @ $(q = 1, 5, \hat{s} = 1.0)$,$(q = 2.5, \hat{s} = 1.5)$, $\tilde{B}_{\rm per}$+$\tilde{B}_{\|\|}$	17
66	NSTX-U STD	k_y @ $q = 1.5, 2.5$, $\beta_e = 0.005$, $\tilde{B}_{\rm per}$+$\tilde{B}_{\|\|}$	22
67	NSTX-U STD	a/L_T @ $a/L_n = 1.0, 2.0$, $\beta_e = 0.005$, $\tilde{B}_{\rm per}$+$\tilde{B}_{\|\|}$	12
68	NSTX-U STD	$\hat{s}$ @ $q = 1.5, 2.0, 2.5$, $\beta_e = 0.005$, $\tilde{B}_{\rm per}$+$\tilde{B}_{\|\|}$	12
69	NSTX-U STD	q @ $\beta_e = 0.001, 0.003$, $\tilde{B}_{\rm per}$+$\tilde{B}_{\|\|}$	12
70	NSTX-U STD	$\nu_{e,i}$ @ $\beta_e = 0.005, 0.020$, $\tilde{B}_{\rm per}$+$\tilde{B}_{\|\|}$	19
Total			208

fluctuations. With the exception of β scan 58, we include the pressure gradient term in the growth rate calculations as discussed in Refs.[16,41]. We exclude any cases where CGYRO predicts MTMs as the most unstable mode since these modes are not resolved with the ballooning mode Hermite basis representation used in TGLF and GFS.

The statistics for all of the EM1 scans are shown in Fig.12. Again, GFS demonstrates the best agreement with CGYRO with an average RMS error in γ of 28.7%. The TGLF errors are 76.3% for the SAT1 version and 39.9% for the SAT2 version. In general, all three models have larger errors when $\tilde{B}_\perp$ is included in comparison with the electrostatic results. The impact of $\tilde{B}_\perp$ is not large, and is generally a stabilizing effect on the ITG/TEM growth rates, compared to the ES result. For example, for the NSTX-U STD case parameters, the growth rate at $k_y = 0.3$ is approximately 17% lower when only perpendicular fluctuations are included.

Next, we will discuss the results for the fully electromagnetic (EM2) dataset where both $\tilde{B}_\perp$ and $\tilde{B}_\parallel$ are included. While the pressure gradient term is stabilizing, we find that the impact of $\tilde{B}_\parallel$ is strongly destabilizing for the KBM modes. Fig. 13 shows the results for a β_e scan (scan 65) at a magnetic shear of $\hat{s} = 1.5$. Examining the CGYRO growth rates (black) we see that above $\beta_e = 0.01$, the KBM is destabilized by $\tilde{B}_\parallel$ with large resulting growth rates. The destabilizing effect of $\tilde{B}_\parallel$ on KBMs was also observed in previous studies obtained using the GYRO code[16] and the GS2 code[42]. When only $\tilde{B}_\perp$ is included (EM1) in the CGYRO calculations (not shown) both the ITG and KBM modes are more stable. The GFS EM1 curve in Fig. 13a and TGLF EM1 in

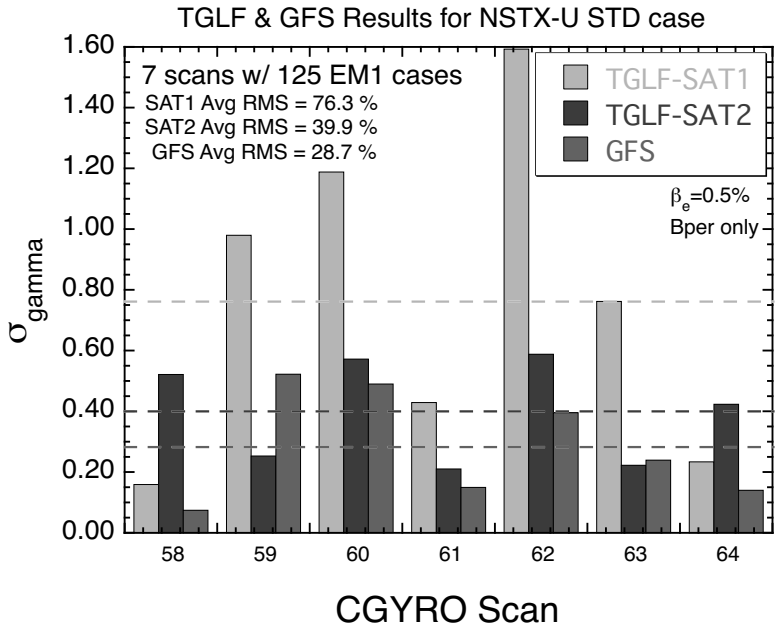

FIG. 12. RMS error in the TGLF and GFS growth rates vs scan number for the CGYRO EM1 database with $(\tilde{\phi}, \tilde{B}_{\perp})$ only.

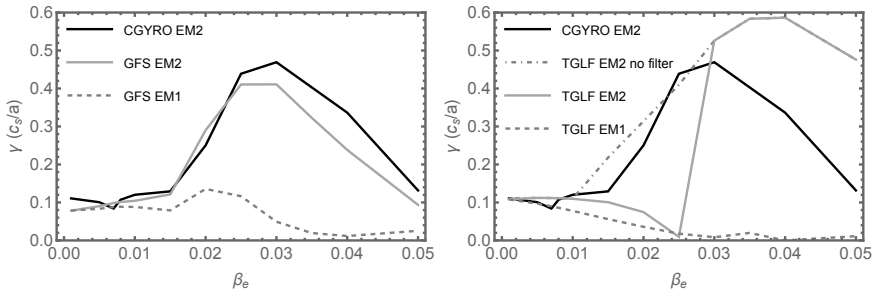

FIG. 13. Growth rate vs β_e for NSTX-U STD case using a magnetic shear of $\hat{s} = 1.5$. Shown are the fully EM results (EM2) for: CGYRO (black), and (a) GFS EM2 (gray) and GFS EM1 (gray dashed) and (b) TGLF-SAT2 EM2 with FILTER=0 (gray dot-dashed) and FILTER=2 (gray) and TGLF-SAT2 EM1 with FILTER=2 (gray dashed)

Fig. 13b (dashed gray) illustrates this result. Comparing the EM2 GFS to CGYRO β_e scan for the NSTX-U STD case in Fig.13a, we find GFS (gray) follows the CGYRO (black) trends very well. In Fig.13b, the EM2 TGLF-SAT2 (gray) has an upshifted threshold for KBM and too large a growth rate at high β_e. The upshift in threshold is caused by the frequency filter applied to TGLF to eliminate spurious modes that sometimes appear below the KBM threshold. Modes with a frequency that is more that 2 times the largest drift frequency are filtered out of the spectrum of TGLF instabilities. The dot-dashed curve in Fig.13b is the result for TGLF-SAT2 without the frequency filtering. In this case, the apparent KBM threshold is at too low a β_e. A filter threshold above 2 would be better for this scan but it may not be optimal for other cases. The default filter of 2.0 was used in all of the NSTX-U STD database runs. No filtering of the modes is applied to GFS.

Comparing the 2 models against CGYRO for the entire EM2 fully electromagnetic dataset in Fig.14, we find that GFS again demonstrates the best agreement with CGYRO. Here, the RMS error in growth rate for the GFS model is 29.2% which is similar to what was found for the EM1 dataset. For TGLF, the RMS errors are 97.4% for the SAT1 version and 52.8% for the SAT2 version. Fig. 14 shows the average errors for each scan.

V. SUMMARY

In this work, three NSTX-U discharges displaying varying mixtures of unstable ITG/TEM, kinetic ballooning (KBM), and micro-tearing (MTM), that were identified from previous gyroki-

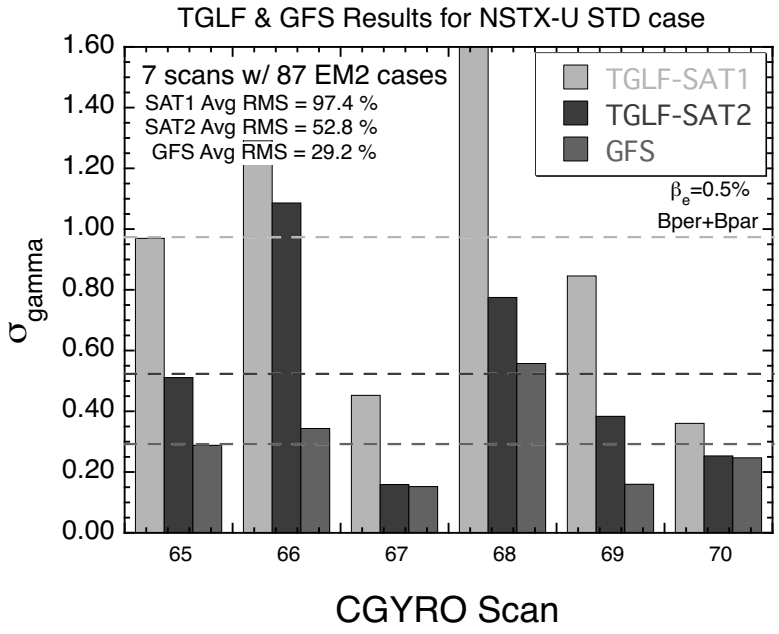

FIG. 14. RMS error in the TGLF and GFS growth rates vs scan number for the CGYRO EM2 database with $(\tilde{\phi}, \tilde{B}_{\perp}, \tilde{B}_{||})$.

netic linear studies, are re-examined with the CGYRO code to study to impact of parallel magnetic fluctuations. This ion-scale mode mixture is noticeably different than what is typically encountered in conventional ($R/a = 3$) tokamaks. As such, this presents a major challenge for driftwave transport models such as TGLF and GFS. Another challenge is that electromagnetic effects can be more important in low aspect ratio discharges. Historically, transport models (e.g. GLF23 and TGLF) have primarily been verified under electrostatic conditions. The results can be summarized as follows:

1. The CGYRO gyrokinetic code has been used for linear stability analysis of three NSTX-U discharges. The senstitivity of long wavelength ITG/TEM modes, kinetic ballooning modes (KBMs), and micro-tearing modes (MTMs) to $\tilde{B}_{||}$ fluctuations was studied.

2. In analyzing the results of the two L-mode discharges, CGYRO shows that, in the deep core, discharge #141716 is KBM dominated while #204551 is MTM dominated. The ion temperature gradient is lower in the MTM dominated discharge and it was found that KBM would be dominant if the ion temperature gradient were increased.

3. Fully electromagnetic CGYRO finds a weakly stabilizing effect on ITG/TEM compared to electrostatic calculations at $k_y = 0.3$. The parallel magnetic fluctuations tend to cancel the stabilizing effect of the perpendicular magnetic fluctuations on ITG/TEM modes.

4. CGYRO analysis finds a strongly destabilizing effect on the KBM due to parallel magnetic fluctuations. This is consistent with previous studies[14–16].

5. CGYRO analysis of discharges with MTMs as the dominant mode found that the MTMs are insensitive to $\tilde{B}_{||}$, unlike the KBM.

6. A low aspect ratio database of linear gyrokinetic runs has been created using the CGYRO code to test the accuracy of the reduced models TGLF and GFS. The database is comprised of parameter scans around a standardized set of NSTX-U-like parameters. It is separated into three groups, an electrostatic (ES) group and two electromagnetic groups EM1 with only $\tilde{B}_{\perp}$ magnetic fluctuations, and EM2 which has both $\tilde{B}_{\perp}$ and $\tilde{B}_{||}$ magnetic fluctuations. The entire database focuses on low-k ITG/TEM and KBM modes. MTMs are not considered

since they cannot be resolved by TGLF or GFS due to the eigenmode representation. It is planned to add a parallel grid, like in CGYRO, to GFS so that MTM can be resolved.

7. The TGLF and GFS models have been verified against the CGYRO database and, overall, the GFS model exhibits the best agreement with both the electrostatic and electromagnetic groups. We find that GFS captures the strong destabilizing effect of $\tilde{B}_{\parallel}$ on the KBMs predicted by CGYRO. On the other hand, TGLF, with or without a frequency filter, struggles to capture the effects of $\tilde{B}_{\parallel}$.

8. When comparing the SAT1 and SAT2 versions of TGLF against the linear CGYRO database we find that the SAT2 version of TGLF is more accurate than the SAT1 version. Both TGLF versions have poorer fidelity to CGYRO than GFS for this ST database test.

ACKNOWLEDGMENTS

This material is based upon work supported by the U.S. Department of Energy, Office of Science, Office of Fusion Energy Sciences, Theory Program and the NSTX-U Research Program, using the NSTX-U Fusion Facility, a DOE Office of Science user facility. We thank the NSTX-U experimental team for providing the data analyses as well as S. Kaye, W. Guttenfelder, and G. Avdeeva for their discussions and assistance.

REFERENCES

[1]G. Staebler, E. A. Belli, J. Candy, J. Kinsey, H. Dudding, and B. Patel, Nucl. Fusion **61**, 116007 (2021).

[2]B. Patel, Ph.D. thesis, https://etheses.whiterose.ac.uk/id/eprint/28991/, University of York, 2021.

[3]G. M. Staebler, J. E. Kinsey, and R. E. Waltz, Phys. Plasmas **12**, 102508 (2005).

[4]G. M. Staebler, J. E. Kinsey, and R. E. Waltz, Phys. Plasmas **14**, 055909 (2007).

[5]G. M. Staebler and J. E. Kinsey, Phys. Plasmas **17**, 122309 (2010).

[6]J. E. Kinsey, G. M. Staebler, and R. E. Waltz, Phys. Plasmas **15**, 055908 (2008).

[7]J. E. Kinsey, G. M. Staebler, J. Candy, R. E. Waltz, and R. V. Budny, Nucl. Fusion **51**, 083001 (2011).

[8]B. Baiocchi, J. Garcia, M. Beurskens, C. Bourdelle, F. Crisanti, C. Giroud, J. Hobirk, F. Imbeaux, I. Nunes, and JET Contributors, Plasma Phys. Controlled Fusion **57**, 035003 (2015).

[9]C. Angioni, T. Gamot, G. Tardini, E. Fable, T. Luda, N. Bonanomi, C. Kiefer, G. Staebler, and the ASDEX Upgrade Team, Nucl. Fusion **62**, 066015 (2022).

[10]M. Ono, S. M. Kaye, Y.-K. M. Peng, G. Barnes, W. Blanchard, M. D. Carter, J. Chrzanowski, L. Dudek, R. Ewig, D. Gates, R. E. Hatcher, T. Jarboe, S. C. Jardin, D. Johnson, R. Kaita, M. Kalish, C. E. Kessel, H. W. Kugel, R. Maingi, R. Majeski, J. Manickam, B. McCormack, J. Menard, D. Mueller, B. A. Nelson, B. E. Nelson, C. Neumeyer, G. Oliaro, F. Paoletti, R. Parsells, E. Perry, N. Pomphrey, S. Ramakrishnan, R. Raman, G. Rewoldt, J. Robinson, A. L. Roquemore, P. Ryan, S. Sabbagh, D. Swain, E. J. Synakowski, M. Viola, M. Williams, J. R. Wilson, and NSTX Team, Nucl. Fusion **40**, 557 (2000).

[11]J. Menard, S. Gerhardt, M. Bell, J. Bialek, A. Brooks, J. Canik, J. Chrzanowski, M. Denault, L. Dudek, and D. Gates, Nucl. Fusion **52**, 083015 (2012).

[12]A. Sykes, R. J. Akers, L. C. Appel, E. R. Arends, P. G. Carolan, N. J. Conway, G. F. Counsell, G. Cunningham, A. Dnestrovskij, Y. N. Dnestrovskij, A. R. Field, S. J. Fielding, M. P. Gryaznevich, S. Korsholm, E. Laird, R. Martin, M. P. S. Nightingale, C. M. Roach, M. R. Tournianski, M. J.

Walsh, C. D. Warrick, H. R. Wilson, S. You, and MAST Team, Nucl. Fusion **41**, 1423 (2001).

[13]J. Harrison, R. Akers, S. Allan, J. Allcock, J. Allen, L. Appel, M. Barnes, N. Ben Ayed, W. Boeglin, C. Bowman, J. Bradley, P. Browning, P. Bryant, M. Carr, M. Cecconello, C. Challis, S. Chapman, I. Chapman, G. Colyer, S. Conroy, N. Conway, M. Cox, G. Cunningham, R. Dendy, W. Dorland, B. Dudson, L. Easy, S. Elmore, T. Farley, X. Feng, A. Field, A. Fil, G. Fishpool, M. Fitzgerald, K. Flesch, M. Fox, H. Frerichs, S. Gadgil, D. Gahle, L. Garzotti, Y.-C. Ghim, S. Gibson, K. Gibson, S. Hall, C. Ham, N. Heiberg, S. Henderson, E. Highcock, B. Hnat, J. Howard, J. Huang, S. Irvine, A. Jacobsen, O. Jones, I. Katramados, D. Keeling, A. Kirk, I. Klimek, L. Kogan, J. Leland, B. Lipschultz, B. Lloyd, J. Lovell, B. Madsen, O. Marshall, R. Martin, G. McArdle, K. McClements, B. McMillan, A. Meakins, H. Meyer, F. Militello, J. Milnes, S. Mordijck, A. Morris, D. Moulton, D. Muir, K. Mukhi, S. Murphy-Sugrue, O. Myatra, G. Naylor, P. Naylor, S. Newton, T. O'Gorman, J. Omotani, M. O'Mullane, S. Orchard, S. Pamela, L. Pangione, F. Parra, R. Perez, L. Piron, M. Price, M. Reinke, F. Riva, C. Roach, D. Robb, D. Ryan, and S. a. Saarelma, Nuclear Fusion **59**, 112011 (2019).

[14]B. A. Carreras, L. Garcia, and P. H. Diamond, Phys. Fluids **5**, 1388 (1987).

[15]M. Kotschenreuther, W. Dorland, Q. Liu, M. C. Zarnstorff, R. L. Miller, and Y. R. Lin-Liu, Nucl. Fusion **40**, 677 (2000).

[16]E. Belli and J. Candy, Phys. Plasmas **17**, 112314 (2010).

[17]R. D. Hazeltine, D. Dobrott, and T. S. Wang, Phys. Fluids **18**, 1778 (1975).

[18]J. F. Drake and Y. C. Lee, Phys. Fluids **20**, 1341 (1977).

[19]A. B. Hassam, Phys. Fluids **23**, 2493 (1980).

[20]J. W. Connor, S. C. Cowley, and R. J. Hastie, Plasma Phys. Controlled Fusion **32**, 799 (1990).

[21]J. Dominski, W. Guttenfelder, D. Hatch, T. Goerler, F. Jenko, S. Munaretto, and S. Kaye, Physics of Plasmas **31**, 044501 (2024).

[22]W. Guttenfelder, J. Candy, S. M. Kaye, W. M. Nevins, E. Wang, R. E. Bell, G. W. Hammett, B. P. LeBlanc, and H. Yuh, Phys. Plasmas **19**, 022506 (2012).

[23]W. Guttenfelder, S. Kaye, D. Kriete, R. Bell, A. Diallo, B. LeBlanc, G. McKee, M. Podesta, S. Sabbagh, and D. Smith, Nucl. Fusion **59**, 056027 (2019).

[24]J. R. Ruiz, W. Guttenfelder, A. E. White, N. T. Howard, J. Candy, Y. Ren, D. R. Smith, N. F. Loureiro, C. Holland, , and C. W. Domier, Phys. Plasmas **27**, 22505 (2020).

[25]J. Berkery, P. Adebayo-Ige, H. Al Khawaldeh, G. Avdeeva, S.-G. Baek, S. Banerjee, K. Barada, D. Battaglia, R. Bell, E. Belli, E. Belova, N. Bertelli, N. Bisai, P. Bonoli, M. Boyer, J. Butt, J.

Candy, C. Chang, C. Clauser, L. Corona Rivera, M. Curie, P. de Vries, R. Diab, A. Diallo, J. Dominski, V. Duarte, E. Emdee, N. Ferraro, R. Fitzpatrick, E. Foley, E. Fredrickson, M. Galante, K. Gan, S. Gerhardt, R. Goldston, W. Guttenfelder, R. Hager, M. Hanson, S. Jardin, T. Jenkins, S. Kaye, A. Khodak, J. Kinsey, A. Kleiner, E. Kolemen, S. Ku, M. Lampert, B. Leard, B. LeBlanc, J. Lestz, F. Levinton, C. Liu, T. Looby, R. Lunsford, T. Macwan, R. Maingi, J. McClenaghan, J. Menard, S. Munaretto, M. Ono, A. Pajares, J. Parisi, J.-K. Park, M. Parsons, B. Patel, Y. Petrov, M. Podestà, F. Poli, M. Porcelli, T. Rafiq, S. Sabbagh, Sánchez Villar, E. Schuster, J. Schwartz, A. Sharma, S. Shiraiwa, P. Sinha, D. Smith, S. Smith, V. Soukhanovskii, G. Staebler, E. Startsev, B. Stratton, K. Thome, W. Tierens, M. Tobin, I. Uzun-Kaymak, B. Van Compernolle, J. Wai, W. Wang, W. Wehner, A. Welander, J. Yang, V. Zamkovska, X. Zhang, X. Zhu, and S. Zweben, Nuclear Fusion **64**, 112004 (2024).

[26]D. Kennedy, C. Roach, M. Giacomin, P. Ivanov, T. Adkins, F. Sheffield, T. Görler, A. Bokshi, D. Dickinson, H. Dudding, and B. Patel, Nuclear Fusion **64**, 086049 (2024).

[27]B. Patel, M. Hardman, D. Kennedy, M. Giacomin, D. Dickinson, and C. Roach, Nuclear Fusion **65**, 026063 (2025).

[28]J. Candy, E. A. Belli, and R. V. Bravenec, J. Comput. Phys. **324**, 73 (2016).

[29]E. A. Belli and J. Candy, Plasma Phys. Controlled Fusion **59**, 045005 (2017).

[30]E. A. Belli and J. Candy, Phys. Plasmas **25**, 032301 (2018).

[31]G. M. Staebler, E. A. Belli, and J. Candy, Phys. Plasmas **30**, 102501 (2023).

[32]G. Avdeeva, K. Thome, S. Smith, D. Battaglia, C. Clauser, W. Guttenfelder, S. Kaye, J. McClenaghan, O. Meneghini, T. Odstrcil, and G. Staebler, Nucl. Fusion **63**, 126020 (2023).

[33]Y. Ren, W. Guttenfelder, S. M. Kaye, E. Mazzucato, R. Bell, A. Diallo, C. Domier, B. LeBlanc, K. Lee, M. Podesta, D. Smith, and H. Yuh, Nucl. Fusion **53**, 083087 (2013).

[34]M. Kotschenreuther, G. Rewoldt, and W. M. Tang, Comput. Phys. Commun. **88**, 128 (1995).

[35]R. L. Miller, M. S. Chu, J. M. Greene, Y. R. Lin-Liu, and R. E. Waltz, Phys. Plasmas **5**, 973 (1998).

[36]W. Tang, J. Connor, and R. Hastie, Nuclear Fusion **20**, 1439 (1980).

[37]R. E. Waltz, R. L. Dewar, and X. Garbet, Phys. Plasmas **5**, 1784 (1998).

[38]M. Beer and G. W. Hammett, Phys. Plasmas **3**, 4046 (1996).

[39]J. Candy and R. E. Waltz, J. Comput. Phys. **186**, 545 (2003).

[40]H. Sugama and W. Horton, Phys. Plasmas **5**, 2560 (1998).

[41]J. Candy, Plasma Phys. Controlled Fusion **51**, 105009 (2009).

[42]N. Joiner, A. Hirose, and W. Dorland, Phys. Plasmas **17**, 072104 (2010).